Streaminglike diffusion in the low-dimensional stochastic pump model

G. Corso and A. J. Lichtenberg

Department of Electrical Engineering and Computer Science, and the Electronics Research Laboratory,
University of California at Berkeley, Berkeley, California 94720

In this paper we analyze a diffusion phenomenon in a few-dimensional Hamiltonian system of coupled mappings in which the principal component of diffusion occurs along resonances. The result is that the diffusion can have power-law dependence in coupling parameter μ and be independent of the stochastic parameter K. For the same range of parameters, the usual analytical Arnold diffusion across resonances is dependent on K and can be much smaller than resonance streaming diffusion. The results are used to qualitatively explain recent results in multidimensional coupled standard maps. [S1063-651X(99)09706-8]

PACS number(s): 05.45.−a, 05.60.−k

I. INTRODUCTION

The problem of the dependence between the perturbation parameter of the diffusion in multidimensional Hamiltonian systems is far from being fully understood. The results of Chirikov, calculating the diffusion in two-and-a-half degrees of freedom [1], and applied to two coupled mappings [2,3], have made reasonably accurate predictions of the diffusion rate. The method called the three-resonance model [1], or stochastic pump model for mappings [2], treats the lowest dimensional system that exhibits Arnold diffusion [1,2]. The three-resonance model predicts $D = (\Delta I)^2/t \propto e^{A/\epsilon^{1/2}}$, where ϵ is the perturbation parameter and $A \approx 1$.

If many resonance layers overlap, then the three-resonance model is not adequate to describe the diffusion, which can be much larger than that calculated using a three-resonance model. An upper bound on the diffusion rate has been obtained by Nekhoroshev [4] of the form $D \propto e^{-A/\epsilon^{\gamma}}$ ($A \approx 1$), where for the number of degrees of freedom L, the optimal value of γ has been shown to be $\gamma \simeq L^{-1}$ [5,6]. If L is large, it is clear that an exponentially small diffusion could only hold for very small ϵ, otherwise the exponential factor would be essentially unity. It has been estimated that, for the exponential form to hold, $\epsilon < \epsilon_L \sim (\sigma_o^2/L)^{2L^2}$, where σ_o is the rate of decrease of Fourier coefficients of an analytic perturbation [6]. For L large, this limits ϵ to very small values. Also, an upper bound is related to the fastest local diffusion, while an average global diffusion is controlled by portions of the phase space where the diffusion is slowest.

In a model problem in which many resonances overlap, for $L = 3$, Chirikov *et al.* [7] numerically investigated the scaling of the diffusion with ϵ, finding that it agreed with the upper bound scaling for ϵ small, while it followed the three-resonance model, $\gamma = \frac{1}{2}$, for larger ϵ. However, the important L dependence was not investigated.

Konishi and Kaneko [8] studied global diffusion in a set of coupled mappings, both for which nearest neighbors are coupled and for which there is all-to-all global coupling, with a perturbation parameter K. They investigated the diffusion for $0.2 \leq K \leq 1$, over a range of N, the number of coupled maps. For nearest-neighbor coupling and $N > 3$ the diffusion coefficient D fitted an exponential with the power

of $\epsilon = K$ given by $\gamma \simeq 0.45$ and independent of N. This is close to $\gamma = 0.5$ predicted from a three-resonance model. For global coupling an exponential form did not fit well; for $N = 4$, 5, and 6 they found that $D \propto K^{\gamma}$ with $\gamma \simeq 5$. Using a general analysis similar to that employed to obtain an upper bound to the diffusion, but applied to larger values of ϵ, Chirikov and Vecheslavov [9] have found that the rate of diffusion for L sufficiently large and ϵ not too small behaves as a power law in ϵ, $D \propto \epsilon^{\eta}$, and is independent of L. The value of η can be adjusted by a fitting parameter, which was compared to [8] to obtain a value of $\eta = 6.5$.

The forms of the mapping studied by Konishi and Kaneko [8] do not distinguish how many resonances are driving the diffusion, and do not distinguish the strength of coupling from the nonlinearity. We adopted an alternate procedure of linking standard maps together through a weak-coupling term [3,10]. We investigated various forms, for example,

$$I_{n+1}^1 = I_n^1 + K^1 \sin \theta_n^1 + \mu \sin(\theta_n^1 + \cdots + \theta_n^m),$$

$$\theta_{n+1}^1 = \theta_n^1 + I_{n+1}^1,$$

$$\vdots \qquad\qquad\qquad (1)$$

$$I_{n+1}^N = I_n^N + K^N \sin \theta_n^N + \mu \sin(\theta_n^N + \cdots + \theta_n^{m-1}),$$

$$\theta_{n+1}^N = \theta_n^N + I_{n+1}^N,$$

where K is the nonlinearity parameter, μ the coupling parameter, with $m-1$ explicit couplings, $m \leq N$. For $\mu = 0$ we have N uncoupled standard maps. The structure of the individual maps is nearly unchanged by making the coupling strength μ small, and the number of interacting resonances is controlled through the number of coupling phases. The nonlinearity parameters K^i, $1 \leq i \leq N$, can also be varied independently of the coupling. The mapping equations (1) are

volume preserving and are also reversible, and may or may not have a complete symplectic form, depending on the specific mapping form chosen.

In previous work [3,10] the mappings were numerically integrated, for a large set of initial conditions, chosen to be in the stochastic phase space of the coupled system, for various values of K, μ, m, and N. The action I was allowed to range over all values, to determine the action diffusion $\Delta I_{\rm rms}$. The values of K and μ were chosen to be sufficiently large that the diffusion rate could be determined in a reasonable time (typically 2^{21}–2^{24} iterations per mapping for each initial condition), while μ was chosen sufficiently small so as not to greatly perturb the phase space of the individual maps. The standard map has the useful property of being 2π periodic in both angle and action, so that diffusion can be followed over $\Delta I_{\rm rms} \gg 2\pi$.

The local rate of Arnold diffusion can be calculated, using a generalization of the three-resonance model obtaining good agreement with numerical diffusion over a limited range of m and K [3]. A formula for global diffusion was obtained, using a generalization of phase-space arguments that had been developed to treat a simpler problem [11]. Reasonable agreement between theory and experiment was obtained in initial studies with $K=0.8$. In a subsequent study the K dependence was explored over the range of K between 0.3 and 0.8 and over a large range of m values. The expected μ dependence and power-law numerical results gave K dependence for the diffusion $D \propto \mu^2 K^\beta$, where $1.5 < \beta < 2.5$. Since the studies in [8] varied a single parameter ϵ, combining coupling and nonlinearity, this would correspond in our case to $D \propto \epsilon^4$ ($\beta=2$), somewhat below the value of $D \propto \epsilon^5$ obtained there. Furthermore, our theoretical averaging procedure to obtain the global diffusion produces a dominant scaling of $D \propto \mu^2 K$, such that $D \propto \epsilon^3$. The theory, however, made a very strong assumption on the phase averaging, which should be significantly in error for small m.

In order to explore the reasons for these discrepancies, and to see if there are additional mechanisms leading to the diffusive process, we have explored a simpler system of mappings in which the mappings with stochastic driving phases are decoupled from the driven action and phases. This separation allows much simpler averaging than in our previous work, but at the cost of less symmetry. In Sec. II we introduce the new system and numerically determine the diffusion. In Sec. III we analyze in more detail the new map. Then, in Sec. IV we calculate the diffusion arising from the dominant mechanism. Finally, in Sec. V the conclusions are given.

II. NUMERICAL RESULTS WITH SIMPLIFIED MAPPINGS

We start with a Hamiltonian system (coupled symplectic mappings) perturbed from their action-angle coordinates. Dividing the angles into driving and driven ones, the former are in their stochastic layers, only coupled in one direction through their angles, one to one, with the driven maps, which are in rotational or librational orbits. The driving angles (primed) act like time, although governed by the complicated behavior in a bound separatrix layer. The general mapping system is shown in Eqs. (2),

$$\bar{I}^1 = I^1 + \mu \sin(\theta^1 + \cdots + \theta^N + \theta'_1),$$

$$\bar{\theta}^1 = \theta^1 + \bar{I}^1,$$

$$\vdots$$

$$\bar{I}^N = I^N + \mu \sin(\theta^1 + \cdots + \theta^N + \theta'_N),$$

$$\bar{\theta}^N = \theta^N + \bar{I}^N,$$

$$(2)$$

$$\bar{I}'_1 = I'_1 + K \sin(\theta'_1),$$

$$\bar{\theta}'_1 = \theta'_1 + \bar{I}'_1,$$

$$\vdots$$

$$\bar{I}'_N = I'_N + K \sin(\theta'_N),$$

$$\bar{\theta}'_N = \theta'_N + \bar{I}'_N.$$

As in Eqs. (1), the couplings μ are independent of the primary nonlinear parameter K that drives the diffusion. Although the driven maps can also be in their stochastic layers, the fraction of time (phase space) is very small compared to the fraction of time (phase space) when the driven maps are in rotational or librational orbits. We therefore neglect diffusion arising from the stochastic layer of the driven maps compared to the continuous driving from the stochastic maps.

The mappings (2) diffuse according to the Arnold mechanism, and the local diffusion coefficient depends exponentially with K,

$$D_A = 16\mu^2 Q_o^2 \frac{\exp(\pi Q_o)}{\sinh^2(\pi Q_o)}, \tag{3}$$

where Q_o is the ratio between the frequency of the driven and driving angles [1,3,11]. The single driving angle has frequency $K^{1/2}$, while the driven frequency is the sum of the frequencies of the other angles, mod2π. As described in previous work, if there is only a single driven angle (say θ_1) being driven by θ'_1, then the local diffusion across any ΔI_1, with $\Delta I_1/I_1 \ll 1$, depends on the local frequency of θ_1, which in rotation is just I_1. Thus $Q_o(I_1) = I_1/K^{1/2}$; since I_1 spans the space $0 - \pi$, the diffusion is very slow for I_1 near π and K small. Therefore, we expect the global diffusion to be limited by the slowest diffusion when I_1 is near π. However, if we have additional angles in the phase term, then the value of local $Q_o = (I_1 + I_2 + \cdots + I_N) \bmod 2\pi/K^{1/2}$. With a sufficient number of angles we might expect that for each I_1 the other I's can take on values to make $Q_o = O(1)$ and thus have rapid diffusion everywhere, with only an additional
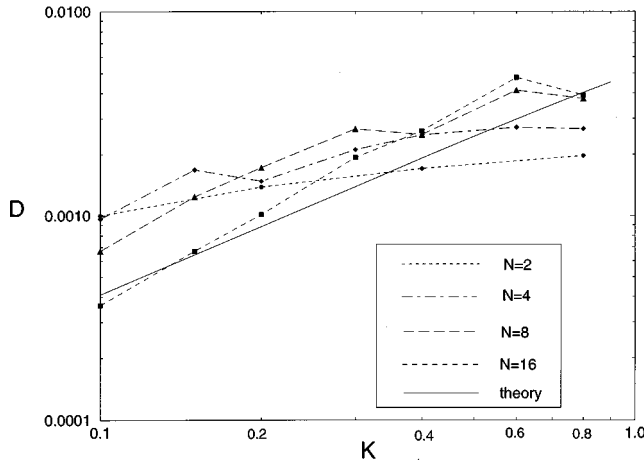
FIG. 1. Comparison of the numerically determined D, from Eqs. (5), as a function of K for various values of N, to the value calculated from the dominant term in the averaging, from Eq. (4); $\mu = 0.1$.

phase-space ratio giving the probability $P(Q_O \sim 1)$. This was done in [10], leading to a dominant term

$$D \approx \frac{2}{\pi} \int_0^\pi \left(4 \frac{I}{K^{1/2}} \frac{\exp[(\pi/2)(I/K^{1/2})]}{\sinh(\pi I/K^{1/2})} \right)^2 dI, \qquad (4)$$

where the integral can be taken to extend over the entire phase space. At small I we expanded $\sinh(\pi I/K^{1/2})$ for small argument, to obtain an approximate scaling $D \propto K$.

As described above, the numerical results gave power laws somewhat larger. In fact, for a small number of phases the averaging assumption leading to Eq. (4) should not be fulfilled, and therefore slower diffusion with a higher power of K would be expected. As K becomes small we would expect that large values of m are required to satisfy the averaging condition.

In Fig. 1 we plot D versus K from Eqs. (2) for $0.1 \leqslant K \leqslant 0.8$ and $\mu = 0.1$ with various values of $m = N$. All results are normalized by the number of initial conditions, and the number of mappings,

$$D = \frac{1}{n} \Delta I_{\mathrm{rms}}^2 = \sum_{i=1}^M [I_i(n) - I_i(n)]^2 / NMn, \qquad (5)$$

where M is the number of initial conditions, usually with $M = 512$, gives good statistics. We have also checked that, after an initial transient, we have normal diffusion, with $\Delta I_{\mathrm{rms}}^2 \propto n$. We see a surprising pattern, with the large N results roughly following the theoretical predictions of Eq. (4), numerically calculated (solid line), while the lower values of N have weaker K dependence. As described above, we would expect stronger K dependence for small values of N, as the phase averaging fails to be complete.

The results indicate that another process is at work, not covered by the previous analysis [3,10]. We have, in fact, encountered such a process, called *resonance streaming*, in which an external stochastic parameter drives two actions along their principal resonance [11,12]. As we shall see below, this process which we have neglected in the previous

Arnold diffusion calculations becomes dominant at small K. This additional diffusion mechanism probability also accounts for the fact that most of the numerical results for small K lie above the dominant large K diffusion solution. The resonance streaming manifests itself most clearly and is most easily calculated for two driven actions on a single resonance.

III. TWO-DRIVEN-MAP SYSTEM WITH ASSOCIATED MAPS

We consider here the simplest set of maps that actualize the stochastic pump model for diffusion in Hamiltonian systems. We have the following maps for two driven angles θ^1, θ^2 and two driving ones θ_1', θ_2':

$$\bar{I}^1 = I^1 + \mu \sin(\theta^1 + \theta^2 + \theta_1'),$$

$$\bar{\theta}^1 = \theta^1 + \bar{I}^1,$$

$$\bar{I}^2 = I^2 + \mu \sin(\theta^1 + \theta^2 + \theta_2'),$$

$$\bar{\theta}^2 = \theta^2 + \bar{I}^2,$$

$$\bar{I}_1' = I_1' + K \sin \theta_1', \qquad (6)$$

$$\bar{\theta}_1' = \theta_1' + \bar{I}_1',$$

$$\bar{I}_2' = I_2' + K \sin \theta_2',$$

$$\bar{\theta}_2' = \theta_2' + \bar{I}_2'.$$

To analyze the streaming diffusion we introduce related maps generated from the sum and the difference driven equations of Eqs. (6). The sum equations give

$$\bar{I} = I + 2\mu \sin\left(\psi + \frac{\theta_1' + \theta_2'}{2} \right) \cos\left(\frac{\theta_1' - \theta_2'}{2} \right),$$

$$\bar{\psi} = \psi + \bar{I}, \qquad (7)$$

where $I \equiv I^1 + I^2$ and $\psi \equiv \theta^1 + \theta^2$ are the new simplectic coordinates. The map (7) in the limit of $K \to 0$ ($\theta_1', \theta_2' \to 0$) becomes the standard map with stochastic parameter 2μ.

Figure 2 shows the distribution normalized to 1 of probabilities Σ of θ_1' and ($\theta_1' - \theta_2'$) for $K = 0.04$. The hyperbolic point is at 0 (2π is equivalent to 0) and the elliptic point at π. As expected, the probability of a particle being close to the hyperbolic point at the vicinity of 0 or 2π is much greater than at π. If both driving angles are in the vicinity of 0 or 2π, ($\theta_1' - \theta_2'$)/2 is approximately 0 or 2π. If one of the driving angles is near 0 and the other near 2π, then ($\theta_1' - \theta_2'$)/2 and ($\theta_1' + \theta_2'$)/2 are near to π. So in the map (7) when both driving angles are in the same vicinity, the value of the cosine function equals approximately 1 and the primed phase in the sine is approximately 0. When the driving angles are not at the same vicinity, the value of cosine equals approximately -1 and $\sin \psi \to -\sin \psi$. In both cases the map (7) behaves like a standard map for most times, i.e., as long as the driving angles stay at the vicinity of 0 or 2π. Figure 2
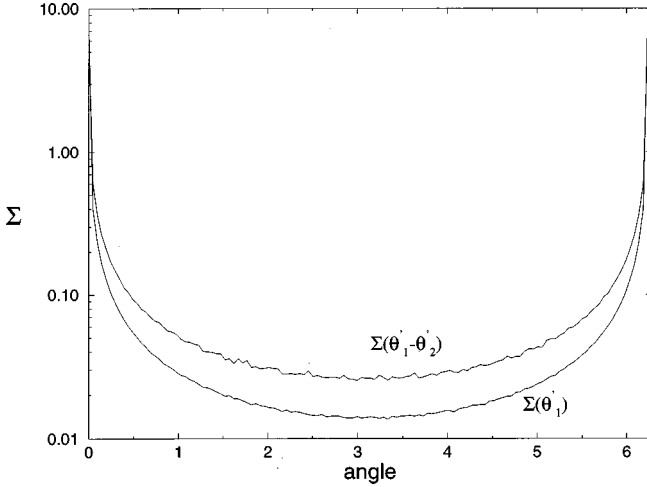
FIG. 2. Distribution of probability Σ, normalized to 1, of θ_1' and $\theta_1' - \theta_2'$ vs angle; $K = 0.04$.

FIG. 3. Graphic of two separatrix angles θ_1', θ_2', in radians, and $\sin[(\theta_1' - \theta_2')/2]$ vs time for $K = 0.02$.

resembles the plot of the distribution of probabilities for a single angle θ_1' in the separatrix. The difference between the distribution of θ_1' and $(\theta_1' - \theta_2')$ is that the distribution close to the elliptic point π is greater in case θ_1' . The reason is that if θ_1' and θ_2' are in the most probable region, close to the hyperbolic point, $(\theta_1' - \theta_2')$ is also around this point, but if at least one of the angles is not there, $(\theta_1' - \theta_2')$ is also not close to the hyperbolic point. We note that the diffusion outside of the resonance will be slow in the sum variable.

To obtain the fast diffusion, we introduce the map created by subtracting the driven equations (6):

$$\bar{J} = J + 2\mu \cos\left(\psi + \frac{\theta_1' + \theta_2'}{2}\right) \sin\left(\frac{\theta_1' - \theta_2'}{2}\right),$$

$$\bar{\psi} = \psi + \bar{I},$$

(8)

where $J \equiv I^1 - I^2$. Note that map (8) is not two degrees of freedom; it is coupled to the dynamic evolution of ψ from map (7). There is a notable difference in the effect of ψ in the sine function of map (7) and in the cosine of map (8). Suppose initially the primed phase of map (7) is near 0 and the ψ phase gives librational orbits which oscillate around π. For $\pi - \alpha < \psi < \pi + \alpha$, we have $-\eta < \sin\psi < \eta$, where $\eta = \sin\alpha$ and α positive. With the same phases in map (8), $-1 < \cos\psi < \sqrt{1 - \eta^2}$. In contrast, for the prime phase of Eqs. (7) near π, $-\beta < \psi < \beta$, also $-\sigma < \sin\psi < \sigma$ in map (8), but $\sqrt{1 - \sigma^2} < \cos\psi < 1$, where $\sigma = \sin\beta$ and β positive. We see that there is an abrupt change in cosine function in map (8) when the primed phase switches from 0 to π. This is responsible for diffusion, as shall be discussed in the next section. Note that $(\theta_1' + \theta_2')/2$ is essentially always equal to 0 or π, except during the relatively short switching time. The streaming is realized in map (8) during the time the term $\sin[(\theta_1' - \theta_2')/2]$ is different from zero. Most of the time $\sin[(\theta_1' - \theta_2')/2] = 0$ because the θ' angles are in the vicinity of the hyperbolic point. But during a time τ the sine term will be close to ± 1 and during that time the term $\cos[(\theta_1' - \theta_2')/2]$ in Eqs. (7) is close to 0 such that $I = I^1 + I^2 \simeq 0$. Then the variable ψ does not oscillate greatly and $J = I^1 - I^2$
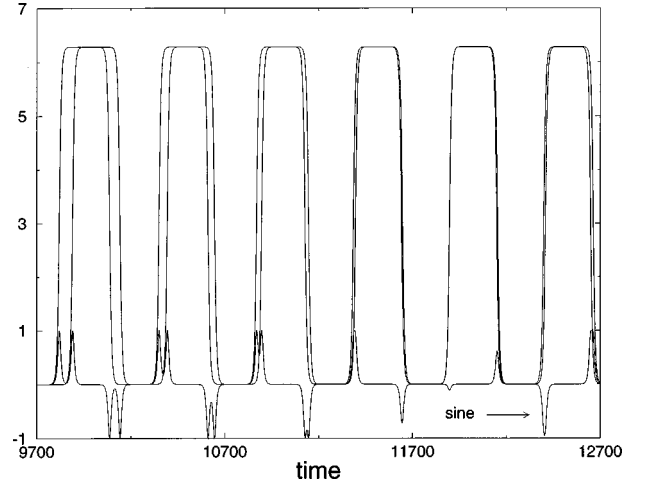
streams during this time τ since the cosine term in map (8) is relatively constant. The streaming of J is therefore proportional to 2μ and a random phase factor.

In Fig. 3 the separatrix angles θ_1', θ_2' and the function $\sin[(\theta_1' - \theta_2')/2]$ are plotted versus time for $K = 0.02$. The peaks in the figure correspond to the small time that $\sin[(\theta_1' - \theta_2')/2]$ is different from zero. The near periodic motion of Fig. 3, which is associated with the average period of the separatrix trajectory T_{av}, as given in [3], is

$$T_{av} \simeq \frac{2\pi^2}{K}.$$

(9)

Each peak of $\sin[(\theta_1' - \theta_2')/2]$ in Fig. 3 corresponds to the transit of the separatrix trajectory from a vicinity of the hyperbolic point from 0 to 2π, or vice versa. The double peaks results from the summing effect between two close transits. For $K = 0.02$, in Fig. 3, $T_{av} \simeq 1000$ corresponding to two oscillations of a separatrix trajectory. Considering that on average there are four peaks for each T_{av}, since there are two angles θ' and one peak for each transit, the average time between peaks ρ is given by

$$\rho = \frac{T_{av}}{P},$$

(10)

where P takes values between 4 and 8, depending on whether the switching of the two angles coincides or not. These can be seen in the figure; we will use $P = 6$ as an average value.

IV. DIFFUSION IN THE SYSTEM OF TWO COUPLED DRIVEN MAPS

To understand the diffusive streaming process, we have to look at the peaks $\sin[(\theta_1' - \theta_2')/2]$ of Fig. 3. In Fig. 4(a) we plot the variable J of map (8) versus time for $K = 0.01$ and $\mu = 0.2$. Figure 4(b) shows, for the same set of parameters and time, the slowly varying $\sin[(\theta_1' - \theta_2')/2]$, the function $\cos[\psi + (\theta_1' - \theta_2')/2]$, which has a rapidly varying and a slowly varying parts, and the product of these two functions. The fast frequency characteristic is $\sqrt{\mu}$ in the cosine function,

(a)

(b)
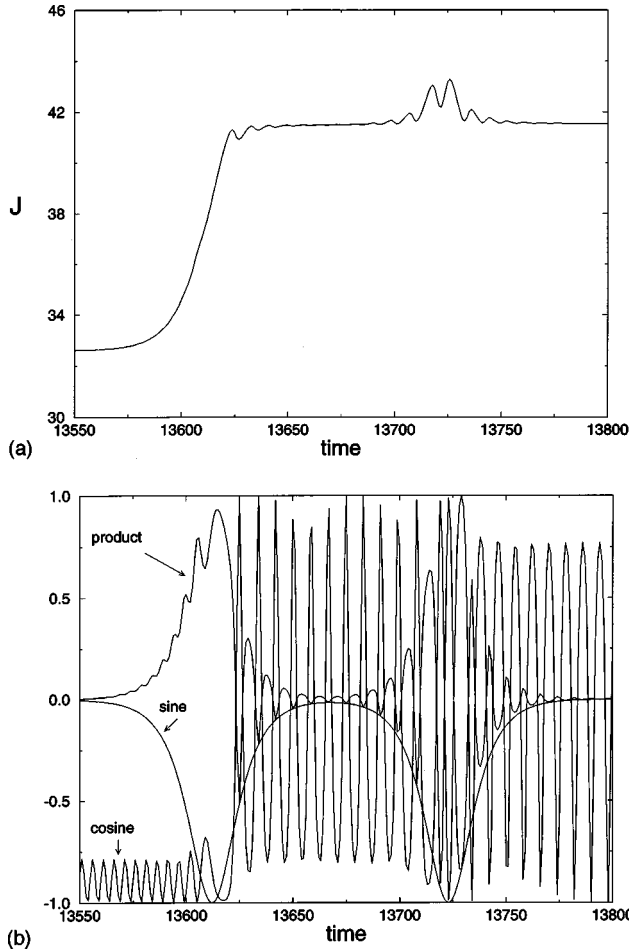
FIG. 4. In (a) the variable J is plotted vs time from Eqs. (8), in (b) functions $\sin[(\theta_1' - \theta_2')/2]$, $\cos[\psi + (\theta_1' - \theta_2')/2]$, and the product of these two functions are plotted; $K = 0.01$ and $\mu = 0.2$.

and the slow frequency characteristic is $\sqrt{K}$ in the sine. As we have commented in the preceding section, the peak causes a change in the cosine phase and values, for instance from $(\theta' - \theta'')/2 = \pi$ and $\sqrt{1 - \sigma^2} < \cos\psi < 1$ to $(\theta' - \theta'')/2 = 0$ and $-1 < \cos\psi < \sqrt{1 - \eta^2}$. The increase ΔJ in map (8), and consequently the diffusion, is proportional to the area over the product function $\cos[\psi + (\theta_1' + \theta_2')/2]\sin[(\theta_1' - \theta_2')/2]$. One can see from the figure that this area is related to the difference $(\eta - \sigma)$. These quantities are difficult to estimate analytically, but can be determined numerically.

The local diffusion coefficient related to the streaming is estimated analogously to the case of diffusion caused by accelerator modes [11]. The variables used are Δl, the mean streaming path, τ, the duration the streaming, and ρ, the time between the peaks, with phase randomization near the hyperbolic points. For Eqs. (8) the main diffusion path is $\Delta l = \tau 2\mu$, the product of the duration of the streaming time τ times the J map step 2μ. The diffusion coefficient

$$D_{\text{local}} = \frac{(\Delta l)^2}{\rho} = \frac{(\tau 2\mu)^2}{\rho}, \tag{11}$$

which is labeled local because it takes place only in that part of phase space where the system is in resonance.

To construct a global diffusion coefficient D we use a phase-space argument as in previous work [2,3,10]:
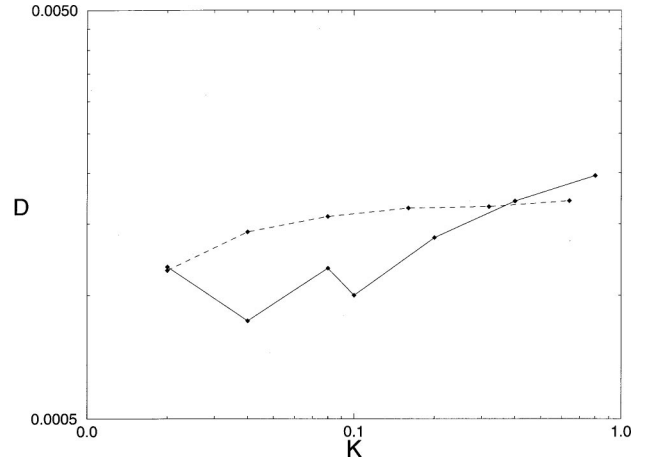
FIG. 5. Solid line is the numerically determined coefficient of diffusion D vs the parameter of stochastisity K, from Eq. (5); the dashed line gives the streaminglike diffusion calculated, from Eq. (14); $\mu = 0.1$.

$$D = D_{\text{local}} \frac{A_{\text{res}}}{(2\pi)^2}, \tag{12}$$

where $(2\pi)^2$ is the total area of the phase space and A_{res} is the resonance area, which can be determined approximately from the pendulum formula to be $A_{\text{res}} \simeq 3\pi\sqrt{2\mu}$.

The time of a peak, from the vicinity of 0 to 2π, or vice versa, is $2\pi/\sqrt{K}$, the orbital period of the pendulum [11]. We estimate the streaming time τ, the center of the peak, by $\tau \simeq 1/\sqrt{K}$. Using this result and Eq. (12) we obtain the following K independent diffusion:

$$D \simeq \frac{\left(\frac{2\mu}{\sqrt{K}}\right)^2}{\frac{2\pi^2}{6K}} \frac{3\sqrt{2\mu}}{4\pi} = 0.29\mu^{2.5}. \tag{13}$$

To numerically estimate the diffusion, we suppose that the streaming is caused basically by the effect of a sequence of single peaks of $\sin[(\theta_1' - \theta_2')/2]$. We evaluate an average $(\Delta l)^2$ in Eq. (11) from a single peak using map (8), where $\theta_2' = 0$ and θ_1' is the separatrix trajectory [11]. Averaging $\Delta l = \Delta J$ over I_0 and ψ_0, for some values of K, and using $P = 4$ corresponding to a single peak in Eq. (10), we write

$$D = \frac{(\Delta l)^2}{P} \frac{A_{\text{res}}}{(2\pi)^2} = \frac{3\sqrt{2\mu}}{2\pi^3} K(\Delta l)^2, \tag{14}$$

whose results we plot with a dashed line in Fig. 5. The solid line plots the coefficient of diffusion obtained from results like those in Fig. 6, for $\mu = 0.1$, where the typical time of 10 million iterations was used. We find reasonable agreement with the predicted K-independent diffusion, and also obtain the magnitude of the diffusion.

In Fig. 6 we plot the dispersion in action, $(\Delta I)^2 \equiv (I_{\text{final}} - I_{\text{initial}})^2$, versus time with $\mu = 0.1$ for $K = 0.4$ and 0.08 for the map (6). The dispersion was computed from the average
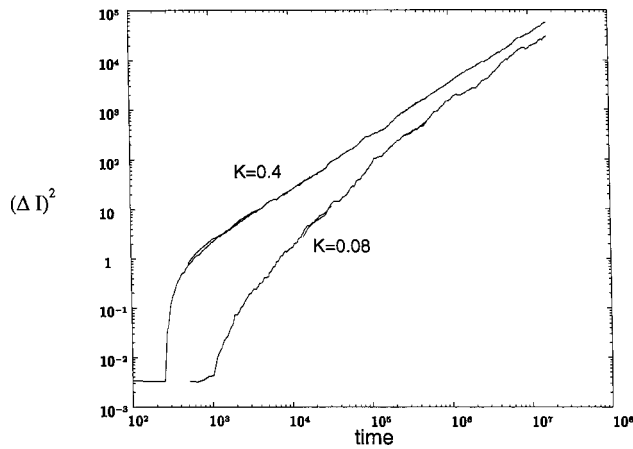
FIG. 6. Log-log plot of the dispersion (ΔI^2) vs time, from Eqs. (7), for $\mu = 0.1$ and $K = 0.4$ and 0.08.

FIG. 7. The numerically determined coefficient of diffusion versus μ, as in Fig. 6, for $K = 0.8$, 0.3, and 0.1.

of 512 particles. The plot shows two distinct transient times before the system attains a diffusive regime. The first is characterized by an initial small constant $(\Delta I)^2$ caused by the initial conditions very close to the hyperbolic point; this is estimated in Eq. (9). The second transient time presents a slope of $(\Delta I)^2$ versus time that is greater than the diffusive, characterizing streaming behavior. This time also increases with decreasing K. These transient times can be observed in the figure.

In Fig. 7 we numerically plot on a log-log scale D versus μ for $K = 0.8$, 0.3, and 0.1. We find an average slope of $D \propto \mu^{2.14}$ which is in reasonable agreement with the value of $D \propto \mu^{2.5}$ found in Eq. (13).

V. CONCLUSIONS AND FINAL REMARKS

We have show that when the stochastic drive of coupled standard mappings is small, then a higher-order diffusion along resonances may be the dominant mechanism for global diffusion. The mechanism, which had previously been studied in problems in which the drive is an external random variable [1,11], was applied here to the case in which the drive is the highly correlated motion within a thin stochastic layer. The physical mechanism was demonstrated in a simple system in which two mappings of mostly regular orbits were coupled together through their phases and also coupled to the phase of a weakly stochastic map which itself is locked in its own stochastic layer. The basic dynamics was exhibited by

transforming the driven maps to sum and difference mappings whose orbits were explored over short times. The results agreed with physical expectations of the diffusive streaming mechanism.

An analytic theory of the diffusion was developed, and the diffusion rate calculated. It was found that the diffusion had the proportionality $D \propto \mu^{2.5}$, where μ is the coupling constant, and was independent of K, the stochastic drive parameter, for K small. These proportionalities were checked numerically over a significant range of μ and K. In fact, the theory and numerics are in good quantitative agreement, as shown in Fig. 5.

Although theory and numerics agreed well for two coupled driven maps, with each coupled to a single driving map, the results are not easily extendible to larger systems. Thus we have found, qualitatively, an explanation for the numerically determined diffusion in Fig. 1, and also for the results in [10]. It may be possible to include this effect, quantitatively, in larger systems, using the type of phase-space argument employed in our previous work [3,10]. This is an interesting avenue for future research.

ACKNOWLEDGMENTS

[1] B. Chirikov, Phys. Rep. **52**, 263 (1979).

[2] J. L. Tennyson, M. A. Lieberman, and A. J. Lichtenberg, in *Nonlinear Dynamics and the Beam-Beam Interaction*, AIP Conf. Proc. No. 57 (AIP, New York, 1979), p. 272.

[3] B. P. Wood, A. J. Lichtenberg, and M. A. Lieberman, Physica D **71**, 132 (1994).

[4] N. N. Nekhoroshev, Russian Mathematical Surveys **32** (6), 1 (1977).

[5] A. Giorgilli, Ann. Inst. Henri Poincaré Phys. Theor. **48**, 423 (1988).

[6] P. Lochack, Phys. Lett. A **143**, 39 (1990).

[7] B. V. Chirikov, J. Ford, and F. Vivaldi, in *Nonlinear Dynamics and the Beam-Beam Interaction* (Ref. [2]), p. 323.

[8] T. Konishi and K. Kaneko, J. Phys. A **23**, L175 (1990).

[9] B. Chirikov and V. V. Vecheslavov, Zh. Eksp. Teor. Fiz **85**, 1132 (1997) [JETP **85**, 616 (1997)].

[10] A. J. Lichtenberg and A. M. Aswani, Phys. Rev. E **57**, 5325 (1998).

[11] A. J. Lichtenberg and M. A. Lieberman, *Regular and Stochastic Motion* (Springer, Berlin, 1983).

[12] J. L. Tennyson, Physica D **5**, 123 (1982).